The Astronomical Journal, 128:3061–3069, 2004 December

LOOKING THROUGH THE HIPPO: NUCLEUS AND DUST IN COMET 2P/ENCKE

David Jewitt
Institute for Astronomy, University of Hawaii, 2680 Woodlawn Drive, Honolulu, HI 96822; jewitt@hawaii.edu
Received 2004 August 6; accepted 2004 September 10

ABSTRACT

We present high-resolution continuum imaging of comet 2P/Encke taken using the Hawaii Imaging Photo-Polarimeter (HIPPO). We measure the brightness, color, and polarization of the dust coma and nucleus at 22°, 93°, and 100° phase angles. At 22° phase angle and 1.4 AU heliocentric distance, the comet appears pointlike in narrowband continuum filters and is unpolarized. In contrast, at phase angles 93° and 100° and ∼0.9 AU heliocentric distance the nucleus appears embedded in a fan-shaped coma that is highly polarized. We find that the nucleus is redder and less polarized than the adjacent coma, and that it is a highly phase-darkened object. The polarization of the coma increases with projected distance from the nucleus, suggesting a change in the mean scattering properties of the grains on a time-of-flight timescale of ∼1 hr. We suggest that disaggregation of composite, porous grains in the heat of the Sun is a likely cause. The high coma polarization of this optically dust-poor comet violates a previously reported correlation between polarization and optical dust content. We briefly discuss the nature of this correlation.

Key words: comets: general — comets: individual (2P/Encke) — techniques: polarimetric

1. INTRODUCTION

Short-period comet 2P/Encke is one of the most intensively studied of all comets. Its non-Keplerian motions, a reaction to asymmetric, sublimation-induced mass loss, formed the cornerstone of Whipple's (1950) classic model of the physical structure of the cometary nucleus. It is known to be small and dark (effective circular radius 2.4 ± 0.3 km and albedo 0.047 ± 0.023) with a rotational variability on timescales of ∼15 hr and a suggestion of evidence for nuclear precession (Fernández et al. 2000). Compared with recent, bright long-period comets such as C/Hale-Bopp and C/Hyakutake, the short-period 2P/Encke loses mass only slowly. The total mass loss is $2-6 \times 10^{10}$ kg per orbit, mostly in the form of large particles that spread around the orbit and give rise to 2P/Encke's thermal dust trail (Reach et al. 2000). The largest of the ejected particles produce the meteors of the Taurid stream.

Curiously, 2P/Encke is underabundant in small dust particles relative to other comets. Judged in terms of its optical spectrum, it is among the most dust-poor of comets (e.g., Newburn & Spinrad 1985). Gehrz et al. (1989) found weak mid-infrared thermal emission from dust and classified 2P/Encke as IR Type I (see also Gehrz & Ney 1992), meaning that the comet is gas-rich and dust-poor. The latter conclusion cannot literally be true, however, since strong, long-wavelength thermal emission indicates a dust/gas production rate ratio in the range 10 to 30 (Reach et al. 2000; Lisse et al. 2004). Reconciliation of the optical and thermal characterizations is possible if the dust mass in 2P/Encke is carried predominantly by particles much larger than a wavelength. Indeed, the lack of a 10 μm silicate emission feature and the absence of superheat (elevation of the dust temperature above the local blackbody temperature due to wavelength-dependent emissivity) indicate large effective grain radii (5–10 μm according to Gehrz et al. 1989, and over 20 μm according to Lisse et al. 2004). 2P/Encke is optically dust-poor because optically bright micron and submicron sized dust particles are underabundant in its coma. Why this is so is unknown. It is speculated that the strange size distribution in 2P/Encke (and in other IR Type I comets) is a result of progressive thermal evolution ("cometary aging"), although the relevant physics remains unspecified.

In this paper, we use narrowband continuum filter data to study the surface brightness, polarization, and color properties of 2P/Encke. Our interest is motivated by the desire to compare the properties of this optically dust-poor comet with those of better studied dust-rich comets. In particular, we are interested in the report by Levasseur-Regourd et al. (1996) that the polarizations of comets are related to their optical dustiness, with the least dusty comets being the least polarized. If this correlation holds true, we should expect to find that 2P/Encke exhibits low optical polarization. More importantly, polarization could represent a powerful tool for the classification of comets by the nature of their dust, if the correlation is real.

2. OBSERVATIONS

Observations were taken at the University of Hawaii 2.2 m diameter telescope on Mauna Kea, Hawaii. The detector was a Tektronix 2048 × 2048 pixel CCD with 24 μm pixels. At the f/10 Cassegrain focus, this CCD gave an image scale of 0.″219 pixel^{-1} and a field of view approximately 7.′5 on a side.

The Hawaii Imaging Photo Polarimeter (HIPPO) was used to detect linear polarization across the field of the Tektronix CCD. HIPPO consists of an electronically controlled rotator assembly that carries a 150 mm diameter polarizing plate constructed by Oriel Instruments (Knopp & Chambers 1997; Chambers 2003). The crossed-polarizer extinction of HIPPO is 10^{-4}. The high throughput of the polarizer (38%) in the *R* band (wavelength ∼6500 Å) allows polarization measurements of astronomically faint targets: the primary intended use is to study polarization in extragalactic sources. The wide field of view makes this polarimeter ideal for measurements of the polarization across extended targets such as cometary comae.

Wavelength discrimination in HIPPO is provided by 100 mm diameter narrowband interference filters from the Hale-Bopp system (Farnham et al. 2000). We used the blue, green, and red continuum filters, known as BC, GC, and RC, respectively. The central wavelengths and full width at half-maximum (FWHM)

TABLE 1
JOURNAL OF OBSERVATIONS

UT (2003)	R[a] (AU)	Δ[b] (AU)	α[c] (deg)	ϵ[d] (deg)	R.A. Rate[e]	Decl. Rate[e]	Scale[f]
Oct 22:06	1.399	0.451	22.1	148	−174.5	57.0	329
Nov 21:06	0.938	0.266	92.9	72	−342.2	−278.9	194
Nov 23:06	0.904	0.273	99.8	65	−320.9	−277.3	199

[a] Heliocentric distance.
[b] Geocentric distance.
[c] Phase angle.
[d] Solar elongation.
[e] Angular rates in right ascension and declination (arcsec hr^{-1}).
[f] Linear scale (km arcsec^{-1}).

transmission of these filters are BC, 4453 ± 61 Å; GC, 5259 ± 52 Å, and RC, 7133 ± 53 Å.

Basic calibration of the CCD images was obtained using measurements of the bias level and flat field obtained by exposing on an illuminated patch inside the observatory dome. No correction was made for dark current, since at the −100°C operating temperature of the CCD, this is negligible. Photometric calibration was obtained using the primary solar analog HD 217014 (51 Peg), which is of spectral type G2.5 IVa and has $m_V = 5.47$, $m_{BC} = 5.943 \pm 0.005$, $m_{GC} = 5.434 \pm 0.005$, and $m_{RC} = 4.668 \pm 0.005$ (Farnham et al. 2000). The polarization standard BD 64°106 (spectral type B1 V, $m_V = 10.34$, V-band linear polarization $p = 5.65\% \pm 0.05\%$; Turnshek et al. 1990) was also observed. Both standards required integration times too short for the reliable operation of the shutter, so we defocused the telescope in order to avoid saturation and nonlinearity effects. Because of our concerns about our ability to accurately recover the flux in defocused imaging data, we experimented with different degrees of defocus and different exposure times. The recovered fluxes were found to be reproducible at the ≤0.5% level. Measurements of the flattened polarization data on BD 64°106 gave $p_{5259} = 5.0\% \pm 0.5\%$, confirming our ability to measure polarization on this bright source. Measurements of random high Galactic latitude field stars gave $p_{5259} = 0 \pm 1\%$, as expected for unpolarized sources.

Observations in 2003 October benefited from a large solar elongation and long observational window (Table 1). The comet at this time exhibited a pointlike morphology in the continuum filters. The small solar elongation of 2P/Encke in 2003 November (Table 1) forced us to observe the comet at low elevations and limited the amount of time we could spend on the measurements. Furthermore, although the integrated magnitude of 2P/Encke in November was $m_V \sim 7$ (Bensch et al. 2003), most of the light was from resonantly fluorescent gas molecules and rejected by the continuum filters and/or fell outside the field of our detector. This is shown in Figure 1, where we compare a 10 s integration through a broadband "$g + r$" filter (central wavelength 5500 Å and 2800 Å FWHM) that admits gas bands and continuum with an image of the green continuum alone, in a composite image having effective integration time of 4500 s. The displayed intensity in the figure has been scaled to the peak of the nucleus signal, so that the two panels are directly comparable. Figure 1 shows that the coma continuum image in 4500 s is fainter than the gas+dust image from only 10 s. The morphology of the comet is similar in the broadband and dust continuum images, but the latter shows only very faint coma due to sunlight scattered by cometary dust. This is compatible with 2P/Encke's longstanding reputation as an optically dust-poor, gas-rich comet.

The polarization data were taken in sequences at staggered polarizer angles in the order 0°, 90°, 45°, and 135° so as to provide some immunity from systematic, time-dependent drift in the photometry. We repeated this sequence for each filter up to four times, generally ending when the comet reached an air mass 1.8 to 2.0. Each image had 300 s integration and was tracked at 2P/Encke's nonsidereal rate (see Table 1; the rates were adjusted hourly to account for small accelerations caused by diurnal parallax).

In measuring the data, we found that the dominant photometric uncertainties were systematic, rather than random, in nature. One important source of error is due to trailed objects in the background of the comet. In the 300 s integrations from November, 2P/Encke moved with respect to the background by about 23″ (105 pixels). The rapid motion and high density of field stars (Galactic latitude of the comet was near 0° in 2003 November) created a major source of uncertainty in the effective "sky" background for individual images within each polarizer position angle. Attempts to remove the background trails were only partly successful because of the small number of images per polarizer angle and filter. In addition to the problems caused by trailed stars, the continuum surface brightness profile of 2P/Encke was very faint. Measurements within large projected apertures suffered from additional systematic uncertainties in the determination of the background sky level, and, again because of the rapid motion and trailing of background objects, we were unable to use profile corrections to reduce this uncertainty. Despite these observational challenges, we were able to secure unique and useful data on 2P/Encke, as we next describe.

3. RESULTS

3.1. *Surface Brightness*

Flat-fielded, sky-subtracted images taken at each polarizer angle, θ, were combined to form a single image for each polarization, wavelength and epoch. In the October data, the condensed morphology of the image allowed us to employ small photometry apertures, with the sky background determined within a contiguous annulus with inner and outer radii 2.″19 and 3.″29, respectively. In the November data, the comet image was extended and the sky level was determined using an annulus with inner and outer radii 16.″4 and 21.″9, respectively. Experiments showed that the derived photometric results were not sensitive to the choice of the annulus inner and outer radii, except that substantially larger radii increased the size of the uncertainty due to residual flat-field errors, while substantially smaller radii encroached unacceptably on the coma. We use $b_\theta(r)$ to denote the surface brightness measured from sky-subtracted

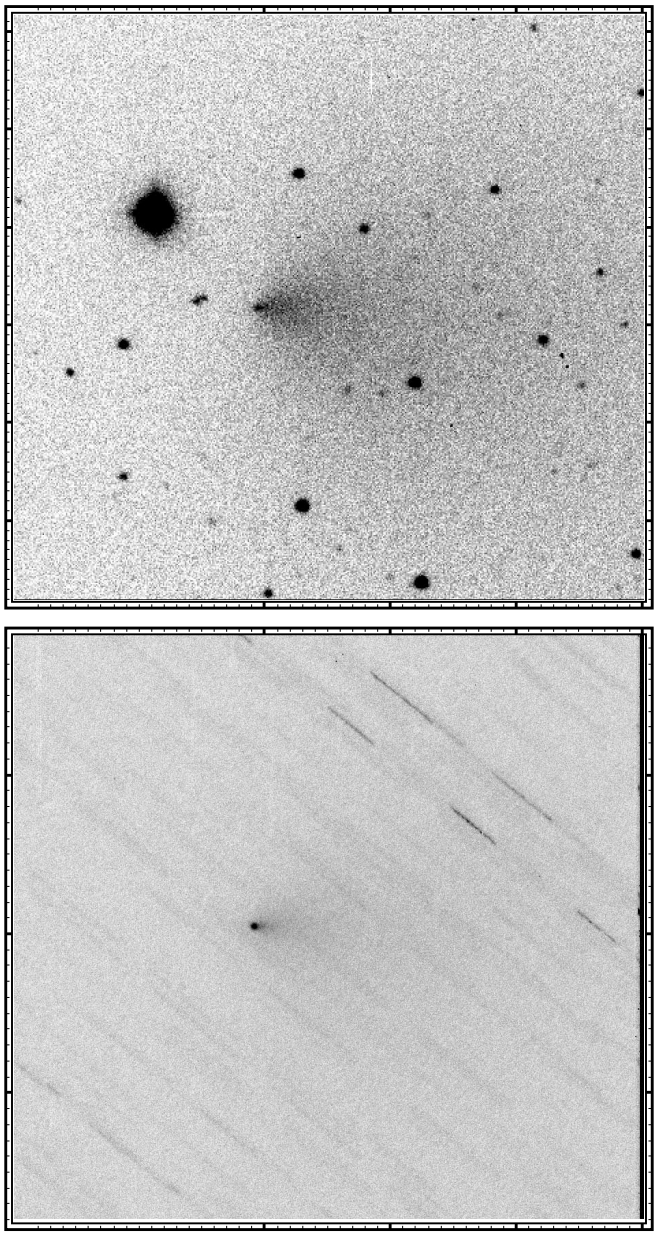

FIG. 1.—Comet 2P/Encke on UT 2003 November 21. *Top*, a single 10 s integration using a broadband "$g + r$" filter taken at 0439; *bottom*, an intensity image compiled from the composite of 15 separate images each of 300 s integration through the GC continuum filter between UT 0454 and 0627. The displays have been scaled to the peak intensity of the nucleus in each image, to directly show the relative strength of the gaseous emission in the broadband filter. The images have north to the top and east to the left, and show a region 200″ wide and 190″ tall (38,800 × 36,860 km at the comet). The Sun is in position angle 238° and the projected heliocentric velocity vector is at 270°.

data within concentric apertures of effective radius, r, at polarizer angle θ. The unpolarized surface brightness was computed from

$$B(r) = \tfrac{1}{2}[b_0(r) + b_{45}(r) + b_{90}(r) + b_{135}(r)]. \quad (1)$$

In images taken in UT 2003 October, the comet appeared morphologically as a point source. Aperture photometry indicates only a minor (few percent) contribution to the total light in the 10 to 15 pixel annulus, consistent with the tail of the point spread function for the data. This observation is in itself remarkable testament to the faintness of the dust in 2P/Encke in October, when at 1.4 AU heliocentric distance. By November, at ~0.9 AU, a sunward fan coma was clearly apparent in addition to a still morphologically pointlike image core. Sekanina (1979) has interpreted cometary sunward fans in general as cones of emission produced when a high-latitude source on the Sun-facing hemisphere is carried around the rotational pole. In this subsection, we seek to quantify the emission in the sunward fan and to isolate the photometric signal from the nucleus of 2P/Encke.

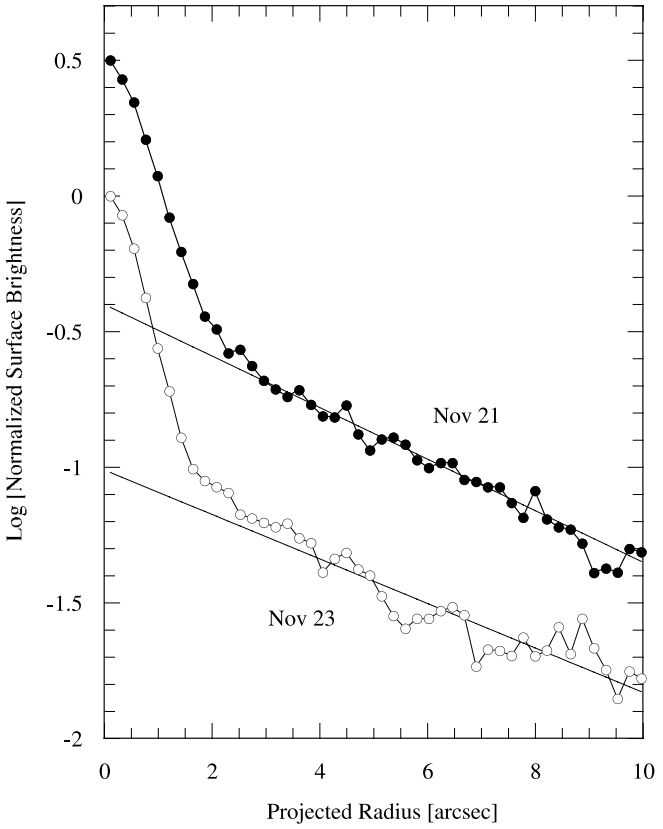

FIG. 2.—Continuum (5259 Å) surface brightness profiles of 2P/Encke computed from the UT November 21 and 23 data. The profiles are vertically offset by 0.5 for clarity. The lines are fits to the coma surface brightness in the 3″ to 9″ projected radius range (see eq. [2]).

Figure 2 shows 5259 Å continuum surface brightness profiles computed according to equation (1). The two curves refer to observations from UT November 21 and 23, as marked, and are normalized to unity at the central pixel. The profile from November 21 has been offset vertically by 0.5 units for clarity. Both profiles consist of a central peak within projected radii ~2″ and an exponential profile at larger radii. The exponential portion is clearly the coma surface brightness profile while the central peak is plausibly attributed to the embedded cometary nucleus. We experimented with two-dimensional convolution models and found that the central excess in Figure 2 cannot be produced as an artifact of the seeing: a source of scattered light in addition to the coma is needed to produce the central excess. However, slight differences in the widths of the central profiles (Fig. 2) are due to differences in the atmospheric seeing on the two nights, with UT November 23 having slightly better seeing than UT November 21.

It is conventional to fit the surface brightness profiles of cometary comae with simple power laws (Jewitt & Meech 1987), but in the case of 2P/Encke, we could not find a convincing

power-law fit. Instead, the coma surface brightness profiles are well fitted by functions of the form

$$\log B(r) = a + \gamma r, \tag{2}$$

where a and γ are constants and $B(r)$ is the normalized surface brightness. Fits to projected radii in the range $3'' \leq r \leq 9''$ are shown in Figure 2 by straight lines. Within the uncertainties, the coma profiles from the two nights were consistent: from the November 21 data we obtained $a = -0.90 \pm 0.02$ and $\gamma = -0.095 \pm 0.003$, while from November 23 we found $a = -1.01 \pm 0.05$ and $\gamma = -0.082 \pm 0.009$. The fits obtained using equation (2) were extrapolated to the cores of the profiles and subtracted to isolate the excess emission in the central peak. In this way, we determined that within apertures of 10 pixels radius the nucleus contributes about 60% ± 5% of the measured optical flux on both nights of observation, corresponding to a magnitude difference $\Delta m_{5259} = 0.55 \pm 0.10$ mag. The quoted error is our best estimate of the uncertainty resulting from the profile fitting and subtraction (e.g., Fig. 2 hints that the coma profile might have a form slightly different from that adopted in eq. [2]).

The surface brightness profile of the coma can be taken to be in steady state when the time of flight for particles crossing the coma is large compared with the timescale for variability in the coma source. A natural cause of variability in the coma source is nucleus rotation, which alters the insolation of exposed volatiles in a periodic fashion. The rotation period of 2P/Encke has been reported near 15.1 hr (Luu & Jewitt 1990; Fernández et al. 2000), although unpublished data suggest that the period may have changed to 11 hr in recent years, or that the nucleus is in a complex spin state with multiple periods (Fernández et al. 2002). For terminal velocities near 0.5 km s^{-1}, representative of micron-sized grains that are dynamically well coupled to the gas flow, the time taken to cross the 10″ ($\sim 2 \times 10^3$ km) region plotted in Figure 2 is on the order of $\tau = 4 \times 10^3$ s, or about 1 hr. This is small compared with the reported rotation periods, meaning that the surface brightness profile of the inner coma cannot be assumed to be in steady state. A nucleus source rotating in and out of sunlight, for example, would drive variable outgassing that would appear in the coma as time-dependent variations in the surface brightness profile. On the other hand, the similarity of the profiles measured on UT November 21 and 23 (Fig. 2) is consistent with steady state.

The surface brightness profile expected from a constant source of dust grains leaving the nucleus at constant velocity is described by the power-law relation $B(r) \propto r^{-1}$. We find that no single power-law fit can adequately represent the coma in the $2'' \leq r \leq 10''$ projected angle range. Instead, the surface brightness gradient becomes steeper with increasing distance from the nucleus. Similarly shaped profiles have been observed in other comets and interpreted as being due to the combined effects of radiation pressure (Jewitt & Meech 1987) and "fading grains" (Baum et al. 1992). Fading grains are grains whose scattering cross section diminishes with time of flight from the nucleus. The effect could be caused by progressive sublimation of uniform particles, or by break-up of aggregate grains into smaller constituent particles whose combined cross sections are less than the cross section of the parent particle. In 2P/Encke, the times of flight across the observed region of the coma are too small for radiation pressure acceleration to play a significant role in creating this downturn in the surface brightness, and so our preferred explanation is that the coma contains fading grains. We will return to this idea in § 4.

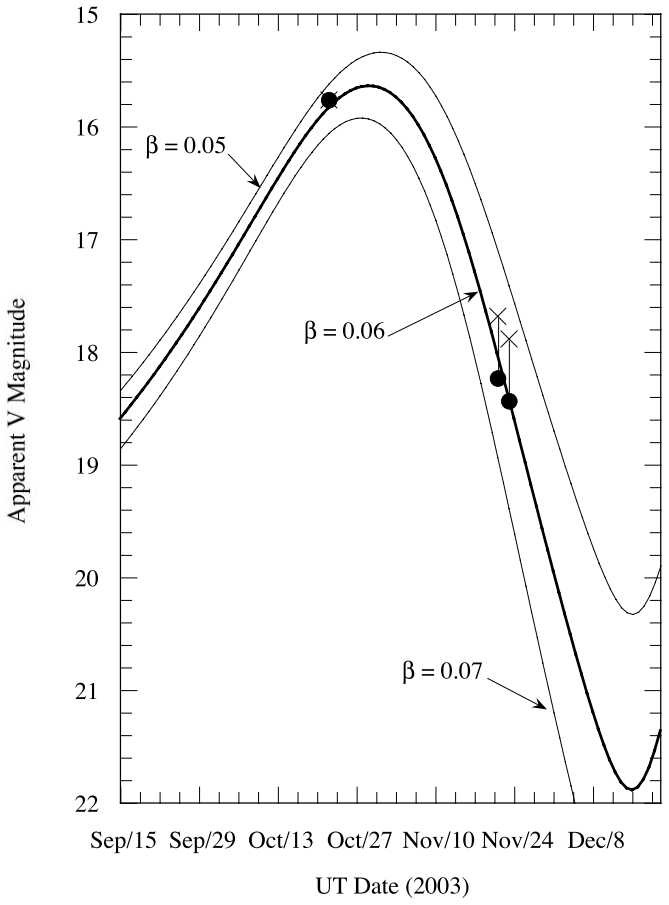

FIG. 3.—Continuum m_{5259} magnitudes as a function of time. Photometry within the central 2.″3 is plotted with crosses. Nucleus photometry, corrected for the presence of coma by the method described in the text, is plotted with filled circles. Lines mark simple models in which the brightness obeys the inverse square law, $V = 15.5 + 5 \log R\Delta + \beta\alpha$, where β [mag deg^{-1}] is the linear phase function and α the phase angle. The three lines show $\beta = 0.05$, 0.06, and 0.07 (mag deg^{-1}).

3.2. *Nucleus Phase Function*

Our first objective is to determine whether or not the nucleus of 2P/Encke was detected in the current observations. One test is to examine whether or not the apparent magnitude varies in accordance with the inverse-square law, once corrected for an appropriate degree of phase darkening and for rotational modulation of the brightness. Most remarkably, the nucleus was *fainter* by ∼2 mag in November than in October despite the fact that the heliocentric and geocentric distances were smaller. We interpret this observation as evidence for phase darkening, since the November data were taken at much larger phase angles than the October data. We fitted the photometry of 2P/Encke with the relation

$$m_V(1, 1, \alpha) = m_V(1, 1, 0) + \beta\alpha, \tag{3}$$

where $m_V(1, 1, 0)$ is the absolute red magnitude of the nucleus, β (magnitudes per degree) is the phase coefficient and α (degrees) is the phase angle. This relation is plotted in Figure 3, together with the nucleus photometry. We see that the new data are very well fitted by $m_V(1, 1, 0) = 15.5 \pm 0.1$ and $\beta = 0.060 \pm 0.005$ mag deg^{-1}. The uncertainty on β is an estimate based on uncertainties on the apparent magnitudes and, especially, uncertainties in the rotational phase of 2P/Encke at the

times of observation. The data closest to ours in terms of phase angle are observations taken with the *Hubble Space Telescope* ($m_R = 17.78 \pm 0.1$ at $\alpha = 106\overset{\circ}{.}2$) as reported by Fernández et al. (2000). From these and other observations, Fernández et al. found $m_R(1, 1, 0) = 15.2 \pm 0.5$ and $\beta = 0.06$ mag deg^{-1} (no uncertainty quoted). Given the color term (see next section) and the photometric uncertainties, we consider that the *Hubble* data and the presently measured absolute magnitudes are in good agreement and both are compatible with the detection of a heavily phase-darkened nucleus.

We note that large phase coefficients are apparently common in the cometary nuclei. For example, 19P/Borrelly has $\beta = 0.05$ mag deg^{-1} (Soderblom et al. 2002), 28P/Neujmin 1 has $\beta = 0.025 \pm 0.006$ mag deg^{-1} (Delahodde et al. 2001), 48P/Johnson has $\beta = 0.059 \pm 0.002$ mag deg^{-1} (Jewitt & Sheppard 2004), and 143P/Kowal-Mrkos has $\beta = 0.043 \pm 0.014$ mag deg^{-1} (Jewitt et al. 2003). In a statistical sense, large phase coefficients are correlated with low geometric albedos, but there is no unique relation between the two. One reason is that for highly aspherical objects like the cometary nuclei (Jewitt et al. 2003), the geometric contribution to the phase coefficient can rival the (albedo dependent) scattering component. Whether the large phase coefficient of the nucleus of 2P/Encke is primarily due to scattering or to body shape and variable perspective is unknown.

3.3. *Color*

The color of 2P/Encke was measured both in October and November of 2003. In October, the large solar elongation of 2P/Encke gave us enough time to measure all three (BC, GC, and RC) continuum filters. Given the absence of coma in the continuum surface brightness profile at this time, we believe that the colors from the October data can be taken to refer to the nucleus. In November, the small solar elongation and rapidly decreasing elevation restricted us to measuring only the GC and RC filters. Moreover, because of time constraints we were able to secure only single images at each polarizer angle when using the RC filter. As a result, suppression of noise and star trails in the derived color profile is less good than in the polarization images presented in § 3.4, for which we have multiple images at each angle. The color data are plotted as differential measurements in Figure 4. We see that the nucleus is redder than the adjacent coma, a property shared with the weakly active Jupiter-family comet P/Tempel 2 (Jewitt & Luu 1989). Presumably, the bluer color of the coma reflects the importance of wavelength dependent scattering from small dust particles.

The nucleus of 2P/Encke is known to show a large rotational variation in its projected cross section (Jewitt & Meech 1987; Luu & Jewitt 1990; Fernández et al. 2000). This temporal variability potentially affects the color measurements because different wavelengths were measured at different times. We used information provided by Y. Fernández (2003, private communication) to estimate the magnitude of the rotational variations of the nucleus in our data. Specifically, we extrapolated from his rotationally resolved photometry obtained in the UT 2003 November 5–9 period to estimate corrections relative to the times of the GC filter measurements. These corrections are small ($\leq$0.1 mag) and they are specifically not the cause of the color difference between the nucleus and coma of the comet. We have included systematic uncertainties due to the rotational variation correction of $\pm$0.05 mag in the following discussion of the color.

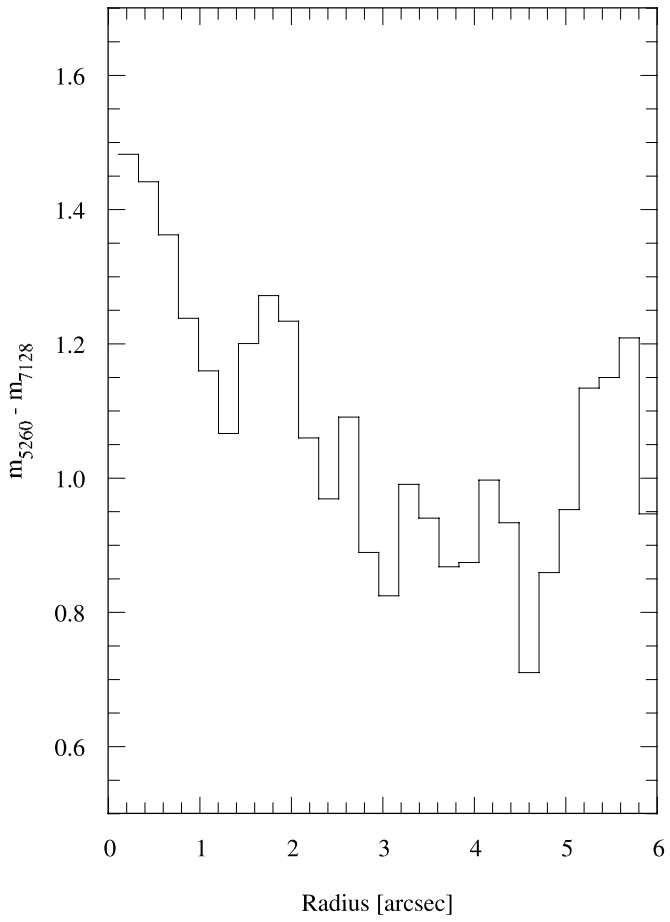

FIG. 4.—Continuum color measured within projected concentric annuli as a function of the annulus radius. The plotted data are from UT 2003 November 23, and the color is measured in the 5259 to 7133 Å wavelength interval.

For comparison with other published works, we calculate the normalized reflectivity gradients, computed from the filter data using

$$S' = \frac{2}{\Delta\lambda}\left(\frac{10^{0.4\Delta m} - 1}{10^{0.4\Delta m} + 1}\right), \quad (4)$$

where $\Delta\lambda$ is the wavelength difference between the filters and Δm is the difference between the color of the comet and the color of the Sun.

Previous measurements of the optical color of 2P/Encke, summarized in Jewitt (2002), have a weighted mean value $S' = 8.9 \pm 1.6\%$ per 1000 Å (corresponding to $m_{GC} - m_{RC} = 0.95 \pm 0.03$). The separate measurements within this weighted mean were all taken at $R \geq 3$ AU and at phase angles between 2° and 13°. This is very close to the measurement of the bare nucleus in 2003 October ($m_{GC} - m_{RC} = 0.96 \pm 0.05$) and slightly bluer than the color extracted from the coma-contaminated data of 2003 November ($m_{GC} - m_{RC} = 1.06 \pm 0.05$). The difference, $\Delta(m_{GC} - m_{RC}) = 0.11 \pm 0.07$, is not formally significant, but we can use it to establish an upper limit to the phase reddening coefficient of the nucleus of 2P/Encke because the October and November data were taken at very different phase angles. The value, $d(m_{GC} - m_{RC})/d\alpha = 1.3 \pm 0.9$ mmag per degree of phase, corresponds to a 3 σ confidence upper bound on the phase reddening at 2.7 mmag deg^{-1} (equivalent to $dS'/d\alpha \leq 0.02\%$ per 1000 Å deg^{-1}). This

TABLE 2
APERTURE POLARIZATION RESULTS

No.	UT (2003)	Filter[a] (Å)	Aperture[b]	m_λ[c]	P[d] (%)
1	Oct 22:06	4453 ± 67	10	16.44	1.5 ± 0.5
2	Oct 22:06	5259 ± 56	10	15.76	1.0 ± 0.5
3	Oct 22:06	7133 ± 58	10	14.80	1.9 ± 0.5
4	Nov 21:06	5259 ± 56	10	17.68	10 ± 4
5	Nov 23:06	5259 ± 56	10	17.88	19 ± 4
6	Nov 23:06	7133 ± 58	10	16.79	...

[a] Central wavelength and FWHM for each filter.
[b] Projected aperture radius in pixels (1 pixel = 0.″219).
[c] Apparent magnitude. The uncertainty on each magnitude is near ±0.05 mag.
[d] Polarization within the projected aperture.

has the same small size (and sign) as the phase reddening estimated for D-type asteroids, 0.04 ± 0.03 %/1000 Å deg^{-1} (Dahlgren et al. 1997). The limited observational evidence thus suggests that phase reddening is not likely to be an important factor in the interpretation of color data pertaining to cometary nuclei, or dark bodies generally, even when taken over a wide range of phase angles.

3.4. *Polarization*

The polarized surface brightness of 2P/Encke is faint enough that we cannot construct useful polarization images at the 0.″219 image scale of the data. Instead, we calculate the circularly averaged polarization from

$$P(r) = \frac{\{[(b_0(r) - b_{90}(r)]^2 + [b_{45}(r) - b_{135}(r)]^2\}^{1/2}}{B(r)}, \quad (5)$$

where $B(r)$ is given by equation (2).

Results from UT 2003 October 22 are consistent with near-zero polarization in each continuum filter (no gas filter polarizations were measured because of time constraints; cf. Table 2). For these measurements we used a 2.″2 radius photometry aperture, but in the absence of coma, the measured values are not sensitive to the aperture employed. Low polarization is an expected consequence of the small phase angle in the October data. Since no coma was apparent in the October data, the measured polarization must refer to the nucleus. For comparison, observations of C-type main-belt asteroids show that the polarization averages ~0.5% at $\alpha = 22^\circ$ (Kiselev et al. 1999): the present data are consistent with this.

The polarization weighted by surface brightness and annulus solid angle is given by

$$P(r_0) = \frac{\int_0^{r_0} 2\pi r p(r) B(r) dr}{\int_0^{r_0} 2\pi r B(r) dr}, \quad (6)$$

and the results are shown in Figure 5. Here $P(r_0)$ is the polarization that would be measured using a circular projected aperture of radius r_0 arcseconds. Results from the two nights in November are plotted in the figure. Within the uncertainties, the two profiles are consistent and so we also plot the average of the data from the two nights. The scatter in Figure 5 can be used to judge the random errors in the polarization data caused by the combined effects of noise, flat-field errors and incompletely removed background sources. An additional systematic error of ~0.5% is present, as determined from standard stars. The integrated polarization is lower than the differential value (Fig. 5) because of averaging within the beam. Values of P measured at larger radii are unreliable because of systematic errors in the surface brightness, which grow rapidly with radius.

Given that only a fraction of the light in the central 2″ emanates from the nucleus (cf. Fig. 3 and § 3.1), we must further correct for near-nucleus coma contamination in order to estimate the nucleus polarization. We used equations (2) and (6) with the polarization versus radius data from Figure 5 to calculate that the integrated polarization of the coma observed in

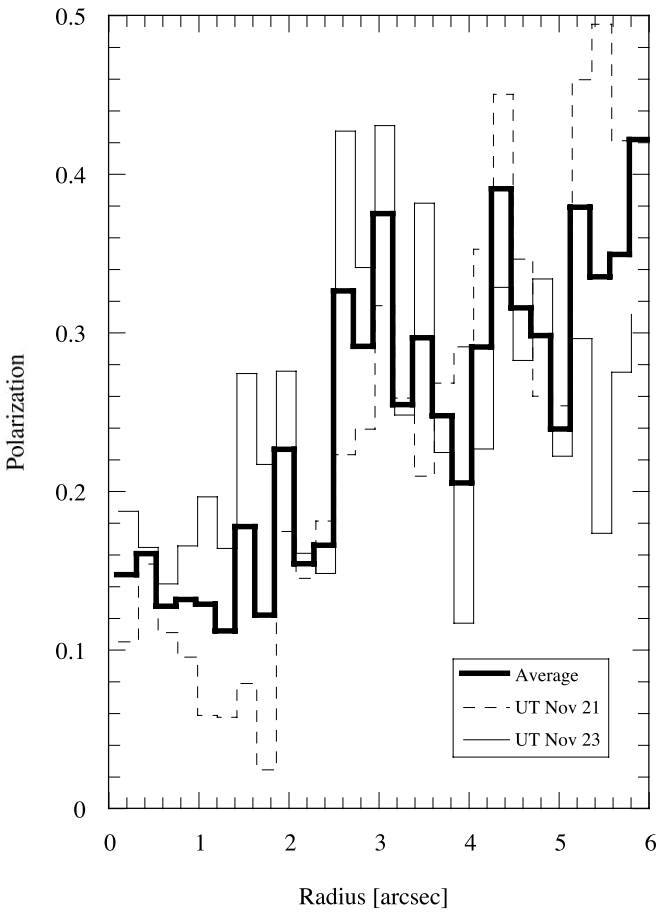

FIG. 5.—Polarization measured differentially at 5259 Å within projected concentric annuli as a function of the annulus radius. Profiles from UT 2003 November 21 and 23 are shown with dotted and solid lines, respectively, while the average is indicated by the thick line. The scatter in the data provides a measure of the random errors on the polarization at each radius. Polarization rises from about 14% in the central 2″ to about 35% at 6″.

isolation within a circle of radius $r = 2''$ would be $P_C(2) = 20\%$. The measured value, including contributions from both the nucleus and the near-nucleus coma, is smaller, $P(2) = 14\%$. Noting that the surface brightness profile requires a nucleus contribution within $2''$ of about 60% (§ 3.1), the derived nucleus polarization in the November data is $P_N = 11\%$. This estimate is uncertain because we do not know how the coma polarization varies spatially inside $2''$ projected radius. To take an extreme case, suppose the coma polarization fell to zero at all projected radii $r \leq 2''$. The implied nucleus polarization would then rise to equal the observed value of 14%. A reasonable estimate of the nucleus polarization is then $P_N = 11\% \pm 3\%$. Regardless of the uncertainties caused by the finite angular resolution of the data, the observation that $P(2) < P_C(2)$ shows that the nucleus cannot be more polarized than the adjacent coma.

Polarization data on other small bodies are few and far between at the high phase angles discussed here for 2P/Encke. The closest comparisons are with near-Earth asteroid 2100 Ra-Shalom (geometric albedo ~0.13), which had *R*-band polarization of 10.7% at phase angle $\alpha = 59.^{\circ}7$ (Kiselev et al. 1999), and with 1685 Toro (geometric albedo 0.14), which had *B*-filter polarization of 7.5% ± 0.1% at $\alpha = 78.^{\circ}5$ (Dunlap et al. 1973). The Martian satellites Phobos and Deimos (albedos 0.06–0.10) have polarizations reported near 20% at $\alpha \sim 80^{\circ}$ (Noland et al. 1973), but these authors allude to potentially significant systematic errors in these data (from the *Mariner 9* spacecraft) and we are uncertain of their reliability. The linear optical polarization of the Moon is related to the albedo of the surface units studied. The lunar highlands (albedo ~0.12) have 90° polarizations ~6%, while the lowlands (albedo ~0.06) have polarizations ~14%, similar to that of the 2P/Encke nucleus (Dollfus & Bowell 1971). In the context of these data, and given its 0.05 ± 0.02 visual geometric albedo (Fernández et al. 2000), the polarization of the nucleus of 2P/Encke does not stand out as unusual.

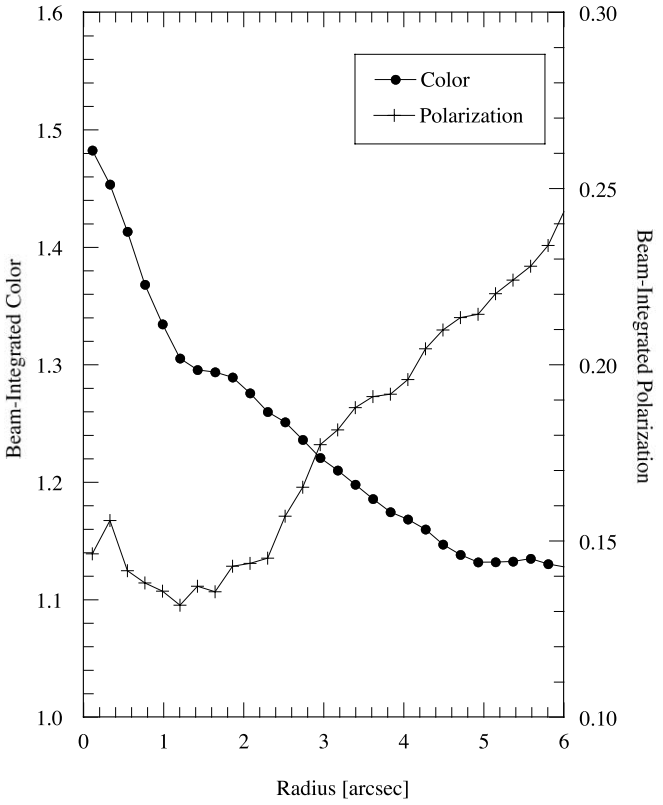

FIG. 6.—Color (in the 5259 to 7133 Å wavelength range) and polarization (at 5259 Å) profiles computed by integrating the differential curves of Figs. 4 and 5. Left and right axes show the color and polarization that would be measured within an aperture as a function of the projected radius of the aperture.

4. DISCUSSION

4.1. *Color and Polarization Gradients*

The average polarization measured at radii above $2''$ samples only the coma and the increase in the polarization with radius must reflect some systematic change in the nature of the dominant scatterers as they leave the near-nucleus environment. Models and experiments show a general trend toward higher polarizations for smaller grain sizes, the limiting case being the Rayleigh limit, in which the polarization can approach 100% (Bohren & Huffman 1983). While size is not the only determinant of polarization (grain composition, shape, structure, and porosity also play a role), it is tempting to think that the gradient in polarization may be produced by a decrease in the mean size of the particles as they recede from the nucleus. Steady shrinkage of the dust grains could be due to sublimation or, more likely, to disaggregation of composite particles bound together by weakly volatile materials. The bluer colors measured at larger projected radii (Fig. 6) would also be consistent with a decrease in the mean grain size with increasing distance from the nucleus. We briefly discuss these effects.

Independent observations suggest that at least some grains in comets are aggregates of smaller particles. This is suggested, for example, by the "bunch of grapes" morphology of the stratospheric particles (Brownlee 1985). These particles, thought to be released from comets, presumably represent the most robust survivors of a population of porous, weakly bonded aggregates. The pore space in these particles might originally have been filled by volatiles that have been lost prior to their collection. Grains in space could be largely held together by volatile, possibly carbon-rich compounds that are destroyed by the heat of the Sun (Lamy & Perrin 1988). Evidence for this disaggregation is provided by impact detectors on spacecraft passing through the comae of comets 1P/Halley and 81P/Wild 2, where the non-Poissonian distribution of impact rates suggests the breakup of parent dust particles after their ejection from the nucleus (Simpson et al. 1986; Tuzzolino et al. 2004). As already remarked, further indirect evidence comes from the surface brightness profiles of the dust comae of comets, some of which show a convex shape that has been interpreted as evidence for "fading grains," possibly due to disaggregation (Baum et al. 1992). The gradient of the coma of 2P/Encke steepens with increasing distance from the nucleus, consistent with fading grains. In the geometric optics limit, the combined cross sections of the component grains produced by disaggregation would exceed the cross section of the initial particle. The observed downturn in the surface brightness requires that the component grains be optically small, such that their individual scattering efficiencies are $Q_s \ll 1$. For nonmetallic grains, this implies effective sizes ≤ 0.1 μm. Fading is also expected from the loss of the "glue" material binding the component grains together. We thus imagine that 2P/Encke releases aggregates of ≤ 0.1 μm particles bound together in aggregates of at least micron size.

At $R \sim 1$ AU, the isothermal blackbody temperature of an exposed grain would be near $T_{BB} = 300$ K. At this temperature the linear rate of sublimation of water ice is $\sim 10^{-7}$ m s^{-1}, so

that a 10 μm ice grain would survive $\sim$100 s. Pure ice grains would have much lower temperatures and longer sublimation lifetimes, but the body of evidence (for example, the nondetection of water ice spectral features in comets at $\sim$1 AU from the Sun) is against the presence of such particles. Materials of higher molecular weight, including certain organics, could sublimate at a rate lower than water (Lamy & Perrin 1988; Boehnhardt et al. 1990). If the grains consist of porous aggregates of particles whose component size is small compared with a wavelength, then temperatures substantially higher than T_{BB} could be reached locally within the aggregate (e.g., Lamy & Perrin 1988 estimate $T \sim 400$ K for 0.1 μm grains at 1 AU). If the aggregates are initially bonded by the volatiles, then exposure to the Sun would lead to disaggregation provided that contact forces, such as the van der Waals force, can be overcome. Differential radiation pressure acceleration and electrostatic repulsion due to charges on the grains caused by photoelectric currents might induce disaggregation following the loss of volatiles (Boehnhardt et al. 1990). A more important effect is centripetal bursting by spin-up from torques imposed by the anisotropic, noncentral loss of volatiles in the sublimating grains. It is easy to show that, to within a small numerical factor, the timescale for rotational spin-up of an aggregate grain is comparable to the timescale for the loss of volatiles from the grain and this is true regardless of the grain size. With no braking mechanism and limited tensile strength, aggregate grains should spontaneously burst when the heat of the Sun drives out their volatile components.

We attempted to use the coma temperature as fitted by Fernández et al. (2000) to estimate the fraction of the solar power used in sublimation from grains in the coma and, hence, to estimate the latent heat. Given the observational and modeling uncertainties, however, we were able to conclude only that the latent heat lies between those of water ($L = 2.2 \times 10^6$ J kg^{-1}) and of graphite ($L = 58 \times 10^6$ J kg^{-1}; Huebner 1970), which is not sufficiently constraining to be of physical interest. A better estimate of the effective latent heat and an observational test of the disaggregating grain model could be made using observations of comets over a range of heliocentric distances. Inside a (latent-heat dependent) critical heliocentric distance, the grains would be warm enough to disaggregate, while outside this distance the aggregates would remain frozen and no polarization or color gradients should be observed. Color and polarization gradients like those observed here should be absent beyond the critical distance, suggesting a simple observational test of the disaggregating grain model. It would also be interesting to model the color and polarization gradients, with a realistic treatment of optical scattering, to determine whether the observed trends (bluer and more polarized with nucleocentric distance) can be quantitatively reproduced (Kimura et al. 2003).

4.2. *Comet Polarization Systematics*

Levasseur-Regourd et al. (1996) have reported evidence for two classes of comets based on measurements of their polarization properties at large phase angles. Their data consist of new measurements obtained using a filter with central wavelength $\lambda = 6700$ Å and full width at half-maximum $\Delta\lambda = 700$ Å combined with previously published measurements obtained with a variety of filters on 23 other comets. They reported that two classes of comet have polarization properties that are similar at phase angles $\alpha \leq 40^\circ$ but divergent at larger angles. Members of the high-polarization class have peak polarization $P_{max} \sim 25\%$–28% at $\alpha \approx 90^\circ$–100° while those of the lower polarization class peak near $P_{max} \sim 15\%$. Moreover, the high-polarization comets are found to be those that are "dusty," whereas the low-polarization comets tend to be "gassy," based on optical spectra.

Based on these two classes, we expect that comet 2P/Encke, with its dust-poor optical spectrum, should belong to the low-polarization comet group ($P_{max} \sim 15\%$). The existence of a strong polarization gradient complicates the characterization of 2P/Encke by a single number. Nevertheless, the differential polarization measurements plotted in Figure 5 are nowhere lower than 15% and grow to $\sim$35% at 6″ projected radius. This supports the report of Kiselev et al. (2004), who used broadband (i.e., gas-contaminated) "continuum" polarization data at smaller phase angles to argue that 2P/Encke might belong to the high-polarization comet group. They measured peak polarizations near 11%, which, when corrected for gas contamination, rise to $\sim$22%. Evidently, 2P/Encke does not fit the polarization classification scheme described by Levasseur-Regourd et al. (1996) in that it is optically dust-poor but nevertheless highly polarized. We note that measurements of very high continuum polarization in C/Hale-Bopp (e.g., Hadamcik & Levasseur-Regourd 2003) have been used to argue that it defines a third polarization class. Are any of these polarization classes real?

The role of polarization gradients deserves further examination. Evidently, not all comets show such gradients (Kelley et al. 2004), but in those that do (like C/Hale-Bopp and 2P/Encke), classification into high- or low-polarization groups may be problematic. In the presence of spatial gradients, the measured polarization must depend on the specific location in the coma that is measured, and so on the angular scale of the measurement and on the geocentric distance to the comet. In this way, biases and sampling artifacts may creep into the data. It is not obvious that spatial gradients would cause cometary polarizations to be divided into two groups, but it is clear that gradients are a potential complicating factor in assigning comets to polarization groups.

A more serious issue concerns contamination of the polarization of the dust by (less polarized) molecular emission lines in data taken using broadband (or poorly optimized continuum) filters (cf. Chernova et al. 1993). Such contamination could easily produce a polarization versus dustiness relation of the type reported. The present, narrowband continuum observations of 2P/Encke are thought to be free of gas contamination. However, of the sources listed by Levasseur-Regourd et al. (1996), several (specifically, Eaton et al. 1991, 1992 and Myers 1985) utilize broadband optical filters that are surely contaminated by molecular line emission. Others (Chernova et al. 1993, 1994; Kikuchi et al. 1989) employ the International Halley Watch continuum filters, which are themselves known to suffer contamination by molecular gas lines (Farnham et al. 2000). Chernova et al. (1993) concluded that molecular contamination explains "a large part" of the difference between high- and-low polarization comets, but not all. Kiselev (1999) has rather bluntly, but probably correctly, concluded that in the study of comets "with rare exception . . . wide band (polarization) observations make no sense." In short, we feel that the reality of the two comet polarization classes remains unclear and the 2P/Encke result (low optical dust and high optical polarization) need not be considered an anomaly. More high-quality continuum polarization measurements near 90° phase are needed to decide whether comet polarizations are really bimodal as opposed to continuously distributed.

5. SUMMARY

High-resolution imaging polarimetry of 2P/Encke at optical wavelengths and two epochs reveals the following:

1. The nucleus appears bare in continuum imaging data from 2003 October (when $R = 1.4$ AU) and is clearly isolated from a surrounding dust coma in data from 2003 November ($R = 0.9$ AU). The phase function and the absolute V magnitude of the nucleus are $\beta = 0.060 \pm 0.005$ mag deg^{-1} and $m_V(1, 1, 0) = 15.5 \pm 0.1$, respectively, from data taken over the 22°–100° phase angle range.

2. The nucleus is redder and less polarized than the adjacent coma. In addition, the coma polarization increases with projected distance from the nucleus, reaching $\sim$35% at $6''$ ($\sim$1000 km) separation and $\sim 100^\circ$ phase angle. The coma becomes more blue with increasing angular distance from the nucleus.

3. The radial variation of polarization and color suggests an evolution of the particle properties on length scales $\sim$1000 km (flight times $\sim$1 hr). Disaggregation of porous, composite grains bound together by weakly volatile material is a likely mechanism.

4. The new polarization data do not fit the standard view of polarization systematics in comets according to which, as described by Levasseur-Rigourd et al. (1996), the least dusty comets have the lowest polarizations. The optical spectrum of comet 2P/Encke is extremely weak in dust but the polarization is high, conflicting with the reported trend.

I greatly appreciate the help provided by Ken Chambers, the owner and feeder of HIPPO, especially his visit to the mountain for initial instrument checkout. I also thank Sean Andrews for help at the telescope. Sean Andrews, Yan Fernández, and Hal Weaver provided comments on the write-up. This work was supported by a grant to D. J. from the NASA Planetary Astronomy Program.

REFERENCES

Baum, W. A., Kreidl, T. J., & Schleicher, D. G. 1992, AJ, 104, 1216
Bensch, F., Bergin, E., & Melnick, G. 2003, IAU Circ. 8249
Boehnhardt, H., Fechtig, H., & Vanysek, V. 1990, A&A, 231, 543
Bohren, C. F., & Huffman, D. R. 1983, Absorption and Scattering of Light by Small Particles (New York: Wiley)
Brownlee, D. E. 1985, Annu. Rev. Earth Planet. Sci., 13, 147
Chambers, K. C. 2003, HIPPO Quick Reference Manual (Honolulu: Inst. Astron., Univ. Hawaii)
Chernova, G. P., Ahmedzyanov, M., & Kiselev, N. N. 1994, Planet. Space Sci., 42, 623
Chernova, G. P., Kiselev, N. N., & Jockers, K. 1993, Icarus, 103, 144
Dahlgren, M., Lagerkvist, C.-I., Fitzsimmons, A., Williams, I. P., & Gordon, M. 1997, A&A, 323, 606
Delahodde, C. E., Meech, K. J., Hainaut, O. R., & Dotto, E. 2001, A&A, 376, 672
Dollfus, A., & Bowell, E. 1971, A&A, 10, 29
Dunlap, J. L., Gehrels, T., & Howes, M. L. 1973, AJ, 78, 491
Eaton, N., Scarrott, S. M., & Gledhill, T. M. 1992, MNRAS, 258, 384
Eaton, N., Scarrott, S. M., & Wolstencroft, R. D. 1991, MNRAS, 250, 654
Farnham, T. L., Schleicher, D. G., & A'Hearn, M. F. 2000, Icarus, 147, 180
Fernández, Y. R., et al. 2000, Icarus, 147, 145
Fernández, Y. R., Lowry, S. C., Weissman, P. R., & Meech, K. J. 2002, BAAS, 34, 887
Gehrz, R. D., & Ney, E. P. 1992, Icarus, 100, 162
Gehrz, R. D., Ney, E. P., Piscitelli, J., Rosenthal, E., & Tokunaga, A. T. 1989, Icarus, 80, 280
Hadamcik, E., & Levasseur-Regourd, A. C. 2003, A&A, 403, 757
Huebner, W. F. 1970, A&A, 5, 286
Jewitt, D., & Luu, J. 1989, AJ, 97, 1766
Jewitt, D., & Meech, K. 1987, AJ, 93, 1542
Jewitt, D., & Sheppard, S. 2004, AJ, 127, 1784
Jewitt, D., Sheppard, S., & Fernández, Y. 2003, AJ, 125, 3366
Jewitt, D. C. 2002, AJ, 123, 1039
Kelley, M. S., Woodward, C. E., Jones, T. J., Reach, W. T., & Johnson, J. 2004, AJ, 127, 2398
Kikuchi, S., Mikami, Y., Mukai, T., & Mukai, S. 1989, A&A, 214, 386
Kimura, H., Kolokolova, L., & Mann, I. 2003, A&A, 407, L5
Kiselev, N. N. 1999, Astron. Vestn, 33, 158
Kiselev, N. N., Jockers, K., & Bonev, T. 2004, Icarus, 168, 385
Kiselev, N. N., Rosenbush, V. K., & Jockers, K. 1999, Icarus, 140, 464
Knopp, G., & Chambers, K. 1997, ApJ, 487, 644
Lamy, P. L., & Perrin, J.-M. 1988, Icarus, 76, 100
Levasseur-Regourd, A.-C., Hadamcik, E., & Renard, J.-B. 1996, A&A, 313, 327
Lisse, C. M., et al. 2004, Icarus, 171, 444
Luu, J., & Jewitt, D. 1990, Icarus, 86, 69
Myers, R. V. 1985, Icarus, 63, 206
Newburn, R. L., Jr., & Spinrad, H. 1985, AJ, 90, 2591
Noland, M., Veverka, J., & Pollack, J. B. 1973, Icarus, 20, 490
Reach, W. T., Sykes, M. V., Lien, D., & Davies, J. K. 2000, Icarus, 148, 80
Sekanina, Z. 1979, Icarus, 37, 420
Simpson, J. A., et al. 1986, Nature, 321, 278
Soderblom, L. A., et al. 2002, Science, 296, 1087
Turnshek, D. A., Bohlin, R. C., Williamson, R. L., II, Lupie, O. L., Koornneef, J., & Morgan, D. H. 1990, AJ, 99, 1243
Tuzzolino, A. J., et al. 2004, Science, 304, 1776
Whipple, F. L. 1950, ApJ, 111, 375